Numerical Methods in Civil Engineering, 9-4 (2025) 01-08

Numerical Methods in Civil Engineering

Journal Homepage: https://nmce.kntu.ac.ir/

Uplift Capacity of Granular Pile Anchors in Clay Using Finite Element Limit Analysis

Amir Hossein Shafiee*, Masoud Oulapour, Zainab Shlaka Drifesh*****

ARTICLE INFO

RESEARCH PAPER

Article history:
Received:
September 2024
Revised:
January 2025
Accepted:
February 2025

Keywords:
Granular pile anchor,
Finite element limit analysis,
Uplift capacity,
Bulging,
Multiple linear regression

Abstract:

The granular pile anchor (GPA) is a relatively new and uncomplicated ground improvement technique that can support tensile loads effectively. In this study, the uplift capacity of GPAs embedded in clay was assessed using finite element limit analysis (FELA) with an adaptive mesh. The analysis considered a broad range of parameters, including the GPA's diameter and length, the undrained shear strength of the surrounding clay, and the friction angle and unit weight of the GPA material. Results showed that the dimensionless uplift capacity generally increased with a higher length-to-diameter ratio. However, the nature of this increase varied for certain cases due to shifts in the failure mechanism of the GPA. Multiple linear regression was applied to establish a practical correlation,, resulting in a predictive equation for dimensionless variables. The model's goodness-of-fit was evaluated using statistical measures such as the z-test, demonstrating its reliability. This study's findings provide valuable insights for designing GPAs in clayey soils and contribute to more effective engineering applications.

1. Introduction

Stone columns are a widely recognized and effective technique for soil improvement. Many studies have been conducted to determine the compressive bearing capacity of stone columns [1-5]. However, stone columns cannot withstand tensile loads because of their granular nature. By installing a plate on the base of the stone column and adding an anchor or tendon to the centre of this plate, the granular pile anchor (GPA) is created to carry uplift loads (Figure 1). Several experimental [6-14], analytical [9], and numerical [10, 15] studies have explored the uplift capacity of GPAs embedded in clay.

One of the first studies on this subject belongs to Kumar and Rao [6], who mentioned that the uplift capacity of GPAs is derived from the weight of the GPA and also, the frictional resistance at the GPA-soil interface.

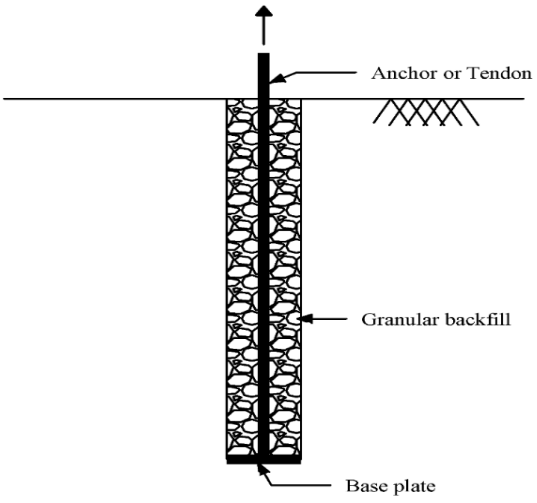

Fig. 1: GPA schematic

Later, Sivakumar et al. [9] conducted several experimental tests to investigate the behaviour of GPAs at failure. They observed that the local bulging mechanism at the base of the

*Corresponding author: Assistant Professor, Department of Civil Engineering, Faculty of Civil Engineering and Architecture, Shahid Chamran University of Ahvaz, Ahvaz, Iran. Email: am.shafiee@scu.ac.ir
**Associate Professor, Department of Civil Engineering, Faculty of Civil Engineering and Architecture, Shahid Chamran University of Ahvaz, Ahvaz, Iran. Email: oulapour_m@scu.ac.ir
***MSc Student, Department of Civil Engineering, Faculty of Civil Engineering and Architecture, Shahid Chamran University of Ahvaz, Ahvaz, Iran. Email: zyneb.sh.2020@gmail.com

https://doi.org/10.61186/NMCE.2409.1074

GPA occurred for longer GPAs with a length-to-diameter ratio greater than 7, whereas shorter GPAs failed due to shaft resistance. Sivakumar et al. [9] also presented the following equation for the shaft resistance of a GPA with diameter D and length L:

$$T_F = \pi DL\alpha C_u + \frac{\pi D^2 L \gamma_g}{4} \quad (1)$$

where T_F is the shaft resistance; C_u is the undrained shear strength of the surrounding clay; γ_g is the unit weight of the GPA's material and α is the adhesion factor. They also presented the following equation for the local bulging capacity (T_B):

$$T_B = \frac{\pi D^2 \sigma_v}{4} \quad (2)$$

where σ_v is the bearing pressure at the GPA base, and can be obtained by:

$$\sigma_v = \frac{1+\sin\varphi}{1-\sin\varphi}(\sigma_{vc} + N_c^* C_u) \quad (3)$$

where σ_{vc} is the overburden pressure, and N^*_c is a bearing capacity factor.

One of the central studies in this field belongs to O'Kelly et al. [10], who determined the uplift capacity of GPAs both experimentally and numerically. They also noted that the failure pattern was influenced by the length-to-diameter ratio of the GPAs. Having plotted the dimensionless uplift versus the L/D bilinear curve, O'Kelly et al. [10] showed that the slope of the shaft resistance section was higher than the local bulging section. Finite element analyses were also conducted to further illustrate the behavior of GPAs. Abishek and Sharma [15] studied the uplift capacity of single and group GPAs and the ground heave using 3-D numerical modeling. They pointed out that the uplift capacity of the GPA increased with a growth in either length or diameter of the pile.

It is worth mentioning that previous numerical studies were limited in scope-often considering only a narrow range of input variables-and did not fully investigate the uplift capacity of GPAs. In contrast, the present study represents the first application of finite element limit analysis (FELA) to this problem, enabling a comprehensive parametric study that considers various values of D, L, C_u, φ, and γ_g. This approach not only fills an existing gap in the literature but also offers a robust and validated methodology for evaluating GPA performance in clay.

In the following sections of this paper, the methodology and problem definition are discussed. Subsequently, the FELA model is verified, followed by a detailed discussion of the results. Finally, concluding remarks are provided. This study is likely the first to apply FELA in investigating the uplift behavior of GPAs.

2. Problem Definition and Approach

The problem consists of a cylindrical GPA with a diameter (D), and length (L), as shown in Figure 2. The center line of the GPA was set as the axis of symmetry. The model dimensions should be selected to ensure that boundary effects are negligible. Thus, we considered a rectangular model with a width of 10 m and a depth of 20 m. In this study, standard boundary conditions, commonly employed in various geotechnical applications [e.g., 16-21] were utilized.

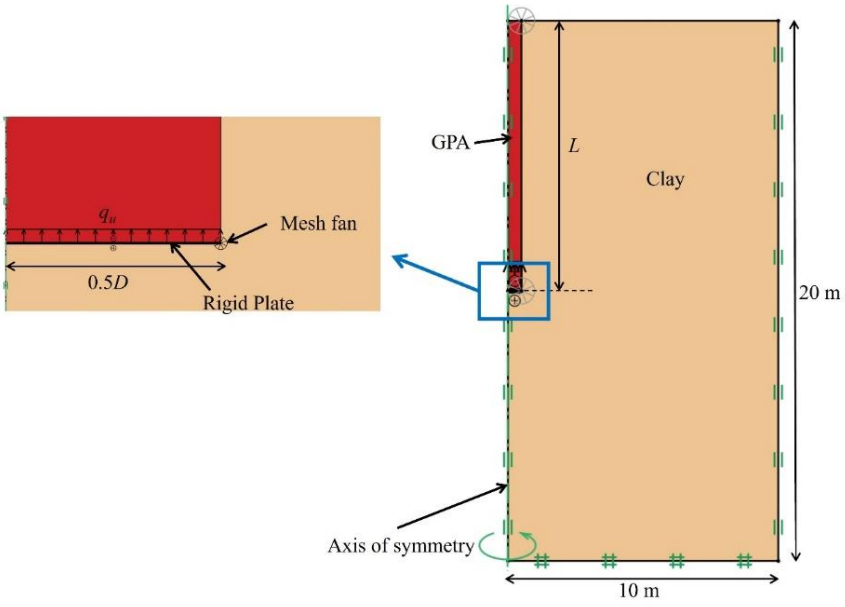

Fig. 2: The FELA model of the problem

In particular, the vertical boundaries were constrained to allow movement only in the vertical direction, whereas the base boundary was fully restrained in both horizontal and vertical directions. This setup is essential because permitting lateral movement at the vertical boundaries can introduce nonphysical deformation modes that alter the actual failure mechanism. By restricting the lateral movement, we ensure that the model accurately captures the intrinsic stability conditions of the system. The Mohr-Coulomb failure criterion was applied to both the GPA material and the surrounding clay. In all cases, the friction angle of the clay was set to zero, indicating that the shear strength of the clay was derived solely from the undrained shear strength, C_u, and no water table, pore-pressure distribution, or seepage effects were considered. This simplification is standard practice for rapid pull-out analyses in cohesive soils [e.g., 9, 15]. Accurately modeling drained uplift response would require coupled consolidation–seepage analyses that account for pore-pressure dissipation and time-dependent deformation, which are beyond the scope of the present FELA framework. Future studies could explore such effects using advanced coupled numerical methods. Although the FELA framework is capable of incorporating more advanced constitutive models, the present study adopts the Mohr-Coulomb model to remain consistent with conventional undrained uplift analyses. Time-dependent behaviors such as creep or thixotropy are beyond the scope of this study. A weightless rigid plate was modeled at the base of the GPA, with the loading represented by an upward distributed load (q_u) applied to this plate. The potential effect of installation-induced disturbance on the surrounding clay was not modeled in this study. Such disturbance could reduce the shear strength of the soil in the vicinity of the anchor. Although this aspect has not been explicitly addressed in previous numerical studies, it remains relevant to practical applications. One possible mitigation approach is to use vibro-displacement techniques for placing granular materials, instead of ramming the aggregates at the base, which may minimize remolding and disturbance in the surrounding clay. The analyses were conducted using the OPTUM G2 finite element limit analysis (FELA) software [22]. FELA offers the capability to handle complex geometries, diverse boundary conditions, and intricate loading scenarios by integrating finite element analysis with limit analysis [23]. A key advantage of FELA over conventional limit analysis methods is that it does not require a pre-assumed failure mechanism [23]. In the present study, multiple mesh configurations were tried at first. Finally, the authors selected an adaptive mesh with 15000 elements, five adaptive iterations, and 1000 start elements. In this mesh setting, the first iteration starts with 1000 elements. In the subsequent iterations, the mesh was refined according to the distribution of plastic shear [22]. The same mesh properties were also used by Shafiee and Eskandarinejad [3] to assess the bearing capacity of stone columns.

A total number of 840 cases were considered as follows:

D = 0.6 m, 1 m

L = 2 m, 4 m, 6 m, 8 m, 10 m, 12 m, 14 m

C_u = 10 kPa, 35 kPa, 60 kPa, 85 kPa, 110 kPa

φ = 35°, 40°, 45°, 50°

γ_g = 18 kN/m^3, 20 kN/m^3, 22 kN/m^3

The values of L and D were selected so that the L/D ratio covered a wide range of values between 2 and 23.3. It is important to note that each case involved two separate analyses: a lower bound and an upper bound. The final solution was determined by taking the average of the upper and lower bound results.

To simplify the analysis, the authors opted to use dimensionless variables, thereby reducing the number of variables involved. These variables were created by applying dimensional analysis as follows:

I) The number of independent variables (N_v) equals six, including q_u, D, L, C_u, φ, and γ_g.

II) The reference dimensions of the variables are as follows: $q_u \doteq [F\underline{L}^{-2}]$; $D \doteq [\underline{L}]$; $L \doteq [\underline{L}]$; $C_u \doteq [F\underline{L}^{-2}]$; $\gamma_g \doteq [F\underline{L}^{-3}]$; and φ is dimensionless, where F and $\underline{L}$ are dimensions of force and length, respectively; and the notation $\doteq$ shows the dimension of the variables. As a result, the number of reference dimensions (N_D) is two, encompassing F and $\underline{L}$.

III) According to the Buckingham Pi theorem [24], the number of dimensionless products (N_p) is 6 – 2 = 4.

The details of the dimensional analysis for the present problem are included in Appendix A. The resulting dimensionless variables were: q_u/C_u; φ; L/D; and $(\gamma_g L)/C_u$. Therefore:

$$\frac{q_u}{C_u} = \mathrm{f}\left(\varphi, \frac{L}{D}, \frac{\gamma_g L}{C_u}\right) \tag{4}$$

The use of the aspect ratio (L/D) as a dimensionless variable has been frequently applied in previous studies [7, 10-12].

3. Verification

Among the numerous pull-out studies available in the literature, only a small subset provided the complete set of essential input parameters—including soil undrained shear strength (C_u) and anchor geometry—necessary for accurate numerical reproduction. To ensure consistency, tests that lacked critical details were excluded from consideration. The authors selected the small-scale experiments of O'Kelly et al. [10] for verification purposes because the required properties for analysis were given in that study. The GPAs

of the experiments were installed in a cylindrical tank with a radius and depth of 2.5 m. The undrained shear strength of the clay inside the tank varied linearly with depth (z) according to: C_u = 64 + 12.5z. The GPAs were made up of compacted gravel with γ_g = 20 kN/m^3, φ = 42°, and a dilatancy angle of ψ = 10°. Table 1 presents the geometric characteristics of the GPAs used in the verification analyses.

Table 1: Verification of FELA solution with the results of experiments of O'Kelly, et al. [10]

Parameter	Case number				
	GA1	GA2	GA4	GA5	GA8
D (m)	0.20	0.20	0.20	0.15	0.15
L (m)	1.2	0.96	1	1.47	1.62
q_u^{FELA} (kPa)	1586.1	1413.3	1457.0	2127.5	2144.0
P_u^{FELA} (kN)[a]	49.8	44.4	45.8	37.6	37.9
$P_u^{O'K}$ (kN)[b]	51	43	47	42.5	42
$\left\|\frac{P_u^{O'K} - P_u^{FELA}}{P_u^{FELA}}\right\| \times 100$	2.4	3.2	2.7	13.0	10.9

[a] $P_u^{FELA} = q_u^{FELA} \times \pi D^2/4$

[b] $P_u^{O'K}$ is the uplift load in kN obtained by O'Kelly et al.[10] experiments

It is important to mention, since the FELA solutions were derived under the assumption of the associated flow rule ($\varphi = \psi$), the modified friction angle (φ^*) as proposed by Davis [25] was applied in the FELA models, as follows:

$$\tan\varphi^* = \eta \tan\varphi \quad (5)$$

where:

$$\eta = \frac{\cos\varphi \cos\psi}{1 - \sin\varphi \sin\psi} \quad (6)$$

The values of φ and ψ of the GPAs of O'Kelly et al. [10] led to φ^* = 36.7°. The verification results are shown in Table 1. The FELA model does not account for soil disturbance during GPA installation or the complexity of soil behavior. As a result, the observed errors were considered acceptable.

4. Results and Discussion

4.1 Parametric Study

The influence of L/D on the uplift capacity of GPAs and the failure mechanism has been a subject of discussion [10, 13]. Figure 3 shows the effect of L/D on q_u/C_u for φ = 35°, 40°, and γ_g = 20 kN/m^3. Two different behaviors are seen in this Figure. For C_u = 10 kPa, the data points followed a relatively linear trend corresponding to the shear resistance mechanism. For higher values of C_u, the data points showed a bilinear trend. As seen in Figure 3, the boundary points between these two linear parts occurred at L/D = 10 and 14 for φ = 35° and 40°, respectively. The shear resistance dominated for L/D values lower than those mentioned above, and the local bulging occurred for higher values with a gentler slope. In general, the bilinear trend of variation of q_u/C_u with L/D was observed for φ = 35°, 40°, C_u = 35 kPa, 60 kPa, 85 kPa, 110 kPa, and all values of γ_g. In contrast, the relatively linear increasing trend was seen for other cases. In other words, the shear resistance mechanism was decisive for the lowest C_u values and highest φ values. This observation coincided with Equations (1-3), as lower C_u values and higher φ values lead to lower shear resistance and higher bulging capacity.

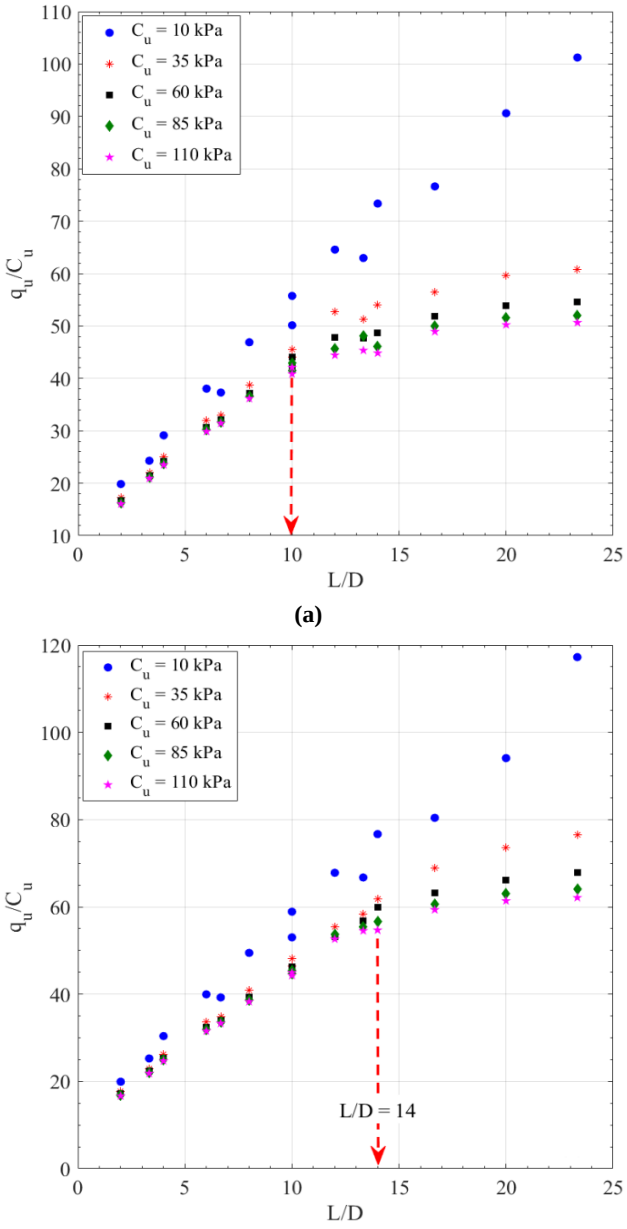

Fig. 3: Variation of q_u/C_u with L/D for γ_g = 20 kN/m^3, and (a) φ = 35°, (b) φ = 40°

The final adaptive meshes of a shear resistance mechanism (φ = 35°, C_u = 35 kPa, γ_g = 18 kN/m^3, L/D = 6.7) and a bulging type mechanism (φ = 35°, C_u = 35 kPa, γ_g = 18 kN/m^3, L/D = 13.3) are shown in Figure 4. Different mesh refinements in these two types of mechanisms are clearly visible. For the shear resistance, the mesh is refined around the base of GPA, where the upward movement occurred, while the mesh refinement covered a larger area beneath and around the GPA for the bulging mechanism.

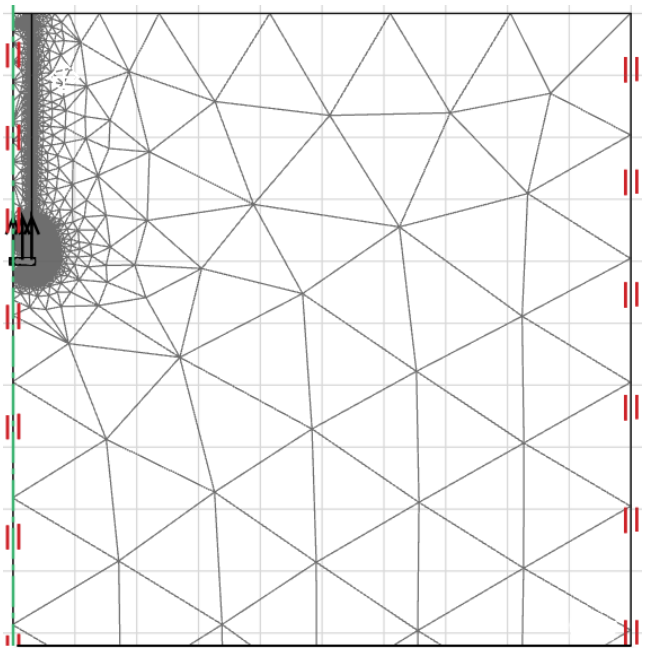

(a)

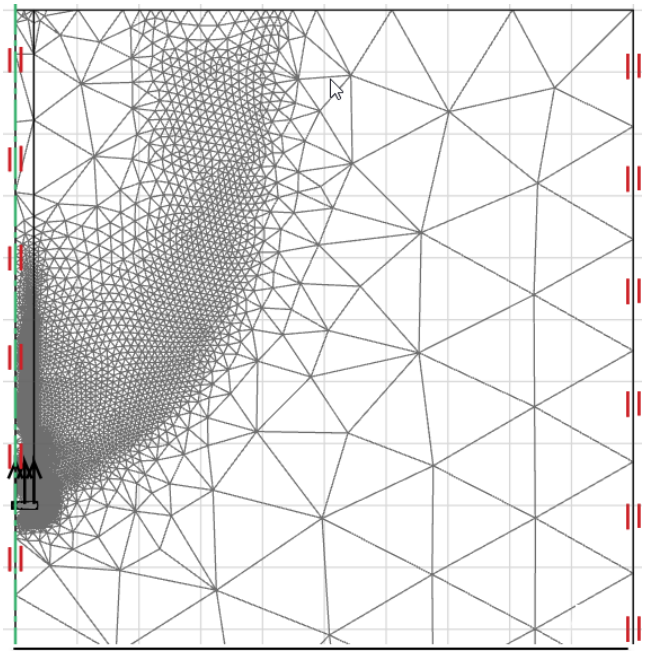

(b)

Fig. 4: Final adaptive mesh. (a) the shear resistance mechanism, (b) the local bulging mechanism

Figure 5 shows the variation of q_u/C_u with φ for different values of $(\gamma_g L)/C_u$. As seen in this Figure, q_u/C_u increased with both φ and $(\gamma_g L)/C_u$ for the shown cases.

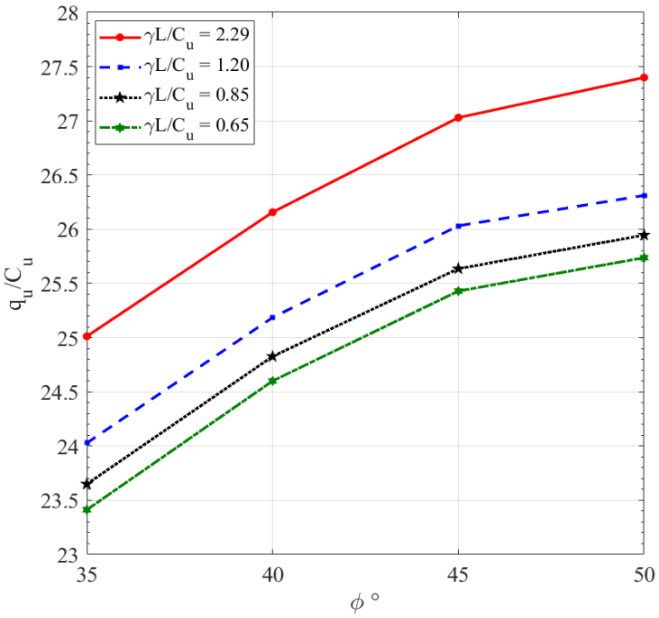

(a)

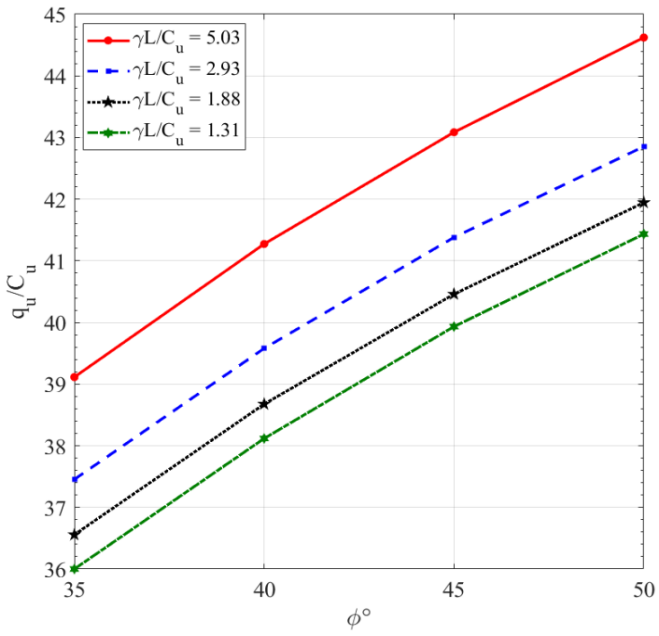

(b)

Fig. 5: Variation of q_u/C_u with φ (a) L/D = 4, (b) L/D = 8

4.2 Model Derivation

In the next step, we implemented a multiple linear regression using an ordinary least squares approach to obtain a model between q_u/C_u as the dependent variable and tan φ, L/D, and $(\gamma_g L)/C_u$, as independent variables. The authors first organi zed their FELA-computed values of q_u/C_u into a response vector and constructed a design matrix that included a

column of ones (for the intercept) and additional columns corresponding to tan φ, L/D, and $(\gamma_g L)/C_u$. The regression then minimized the sum of squared errors between the predicted and computed q_u/C_u values. This process yielded the regression equation:

$$\frac{q_u}{C_u} = 22.5643 \tan\varphi + 2.8052\frac{L}{D} + 0.9609\frac{\gamma_g L}{C_u} - 7.3547 \quad (7)$$

The derived equation exhibited an R^2 value of 0.93. The proposed regression model was developed using data from FELA simulations conducted under short-term, undrained conditions in homogeneous, isotropic clays. It is valid for the given range of parameter variation. Its applicability to layered or non-homogeneous soils has not been investigated. Future research could explore the influence of stratification on uplift behavior through numerical or experimental approaches.

Figure 6 presents a plot comparing the values calculated using FELA with those predicted by Equation (7), alongside the bisector line. The data points are observed to be closely aligned with the bisector line.

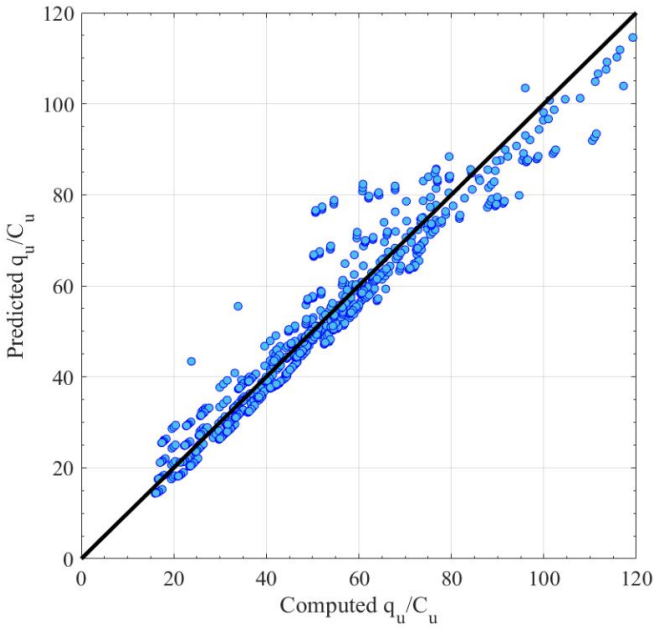

Fig. 6: Scatterplot of the predicted q_u/C_u versus the computed q_u/C_u

Another way of checking the goodness-of-fit of the presented model is to investigate the distribution of normalized residuals. The normalized residuals can be obtained by:

$$\text{Normalized residuals} = \frac{\text{comp}(q_u/C_u) - \text{pred}(q_u/C_u)}{\text{std}(q_u/C_u)} \quad (8)$$

where comp(q_u/C_u) is the computed FELA solution, pred(q_u/C_u) is the predicted value by Equation (7), and std(q_u/C_u) is the standard deviation of computed values.

The normalized residuals must follow a normal distribution function with a mean value of zero and a variance of one, provided that the model fits the computed values perfectly. The histogram and corresponding normal distribution fit of the normalized residuals are shown in Figure 7.

However, visual inspection alone was deemed insufficient. Therefore, the authors conducted a *z*-test to evaluate the null hypothesis that the normalized residuals originated from a normal distribution with a mean of zero and a standard deviation of one. A significance level (α) of 0.05 was adopted. The resulting *p*-value was 0.9974, which is much higher than α, indicating insufficient evidence to reject the null hypothesis.

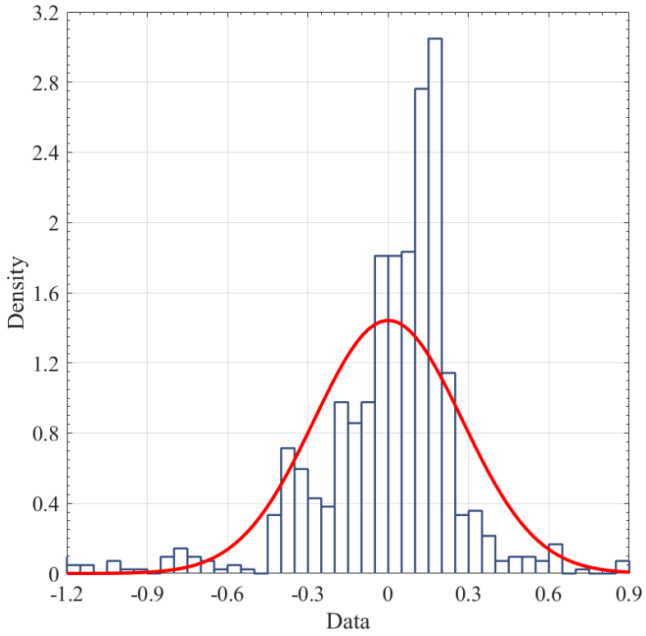

Fig. 7: Histogram of the normalized residuals and the normal distribution fit

5. Conclusions

This study presents a novel application of finite element limit analysis (FELA) to evaluate the uplift capacity of granular pile anchors (GPAs) installed in clay, representing the first effort to employ this method for such a comprehensive parametric investigation. By considering a wide range of input variables (D, L, C_u, φ, and γ_g), our analysis overcomes the limitations of previous studies, which were restricted to narrower parameter ranges. The adaptive FELA approach not only accurately captures the transition between shear resistance and local bulging failure mechanisms but also provides robust predictions that align well with experimental data (as demonstrated in Table 1 against the experiments of O'Kelly et al. [10]). It was observed that:

• In general, the dimensionless uplift capacity (q_u/C_u) increased with the L/D ratio. However, the nature of this

increase varied across cases and depended on the failure mechanism.

• For C_u=10 kPa, the GPAs failed in shear resistance regardless of the values of L/D, φ, or γ_g.

• For C_u >10 kPa and φ = 35° and 40°, the failure mechanism was dependent on the L/D ratio. Higher ratios led to the local bulging mechanism.

Furthermore, the derivation of a statistically validated regression model offers a practical correlation for predicting uplift capacity, with an R^2 value of 0.93 and a supporting residual analysis, confirming the model's reliability. These advances not only enhance the understanding of GPA behavior under uplift loads but also lay the groundwork for future research and improved design practices in geotechnical engineering.

Overall, this work significantly advances the field by introducing a rigorous, versatile, and validated numerical framework that bridges existing gaps in the literature and sets a new standard for evaluating the performance of GPAs in clay.

In practical foundations, granular pile anchors are usually installed in groups rather than as isolated elements. Extending the present FELA framework to simulate multiple GPAs within a single domain would enable quantification of anchor–anchor interaction effect (e.g., overlapping failure surfaces, group efficiency factors, optimal spacing) under undrained conditions. Future studies could focus on such group-interaction analyses.

References

[1] Stuedlein, A. W., & Holtz, R. D. (2013). Bearing capacity of spread footings on aggregate pier reinforced clay. *Journal of geotechnical and geoenvironmental engineering*, 139, 49-58.

[2] Bong, T., Stuedlein, A. W., Martin, J., & Kim, B.-I. (2020). Bearing capacity of spread footings on aggregate pier–reinforced clay: updates and stress concentration. *Canadian Geotechnical Journal*, 57, 717-727.

[3] Shafiee, A. H., & Eskandarinejad, A. (2022). Bearing capacity of single stone column in clay using finite element limit analysis. *European Journal of Environmental and Civil Engineering*, 26, 7958-7971.

[4] Kumar, J., Mukherjee, S. & Pallepati, R.R. (2022). Bearing capacity of circular foundations on weak cohesive soils reinforced with stone columns. *International Journal of Geomechanics*, 22(11), 04022186.

[5] Afshar, J. N., & Ghazavi, M. (2014). A simple analytical method for calculation of bearing capacity of stone-column. *International Journal of Civil Engineering*, 12, 15-25.

[6] Kumar, B. R. P., & Rao, N. R. (2000). Increasing pull-out capacity of granular pile anchors in expansive soils using base geosynthetics. *Canadian Geotechnical Journal*, 37, 870-881.

[7] Rao, A. S., Phanikumar, B., Babu, R. D., & Suresh, K. (2007). Pullout behavior of granular pile-anchors in expansive clay beds in situ. *Journal of Geotechnical and Geoenvironmental Engineering*, 133, 531-538.

[8] Krishna, P. H., & Murty, V. R. (2013). Pull-out capacity of granular anchor piles in expansive soils. *IOSR J. Mech. Civ. Eng*, 5, 24-31.

[9] Sivakumar, V., O'Kelly, B., Madhav, M., Moorhead, C., & Rankin, B. (2013). Granular anchors under vertical loading–axial pull. *Canadian Geotechnical Journal*, 50, 123-132.

[10] O'Kelly, B., Brinkgreve, R., & Sivakumar, V. (2014). Pullout resistance of granular anchors in clay for undrained condition. *Soils and Foundations*, 54, 1145-1158.

[11] Abbas, H. (2020). Laboratory study on reinforced expansive soil with granular pile anchors. *International Journal of Engineering*, 33, 1167-1172.

[12] Sharma, A., & Sharma, R. K. (2021). An experimental study on uplift behaviour of granular anchor pile in stabilized expansive soil. *International Journal of Geotechnical Engineering*, 15, 950-963.

[13] Vashishtha, H. R., & Sawant, V. A. (2021). An experimental investigation for pullout response of a single granular pile anchor in clayey soil. *International Journal of Geo-Engineering*, 12, 1-19.

[14] Joseph, J., Kumar, S., Patel, J.B., Sawant, V. & Tandel, Y. (2022). Model tests on granular pile anchor and helical anchor: A comparative study. *International Journal of Geosynthetics and Ground Engineering*, 8(3), 44.

[15] Abhishek, & Sharma, R. (2019). A numerical study of granular pile anchors subjected to uplift forces in expansive soils using PLAXIS 3D. *Indian Geotechnical Journal*, 49, 304-313.

[16] Keawsawasvong, S., & Ukritchon, B. (2017). Undrained stability of an active planar trapdoor in non-homogeneous clays with a linear increase of strength with depth. *Computers and Geotechnics*, 81, 284-293.

[17] Jamshidi Chenari, R., Zhalehjoo, N. & Karimian, A. (2014). Estimation on bearing capacity of shallow foundations in heterogeneous deposits using analytical and numerical methods, *Scientia Iranica*, 21(3), 505-515.

[18] Khatri, V. N., Kumar, J., & Das, P. P. (2022). Bearing capacity of ring footings placed on dense sand underlain by

a loose sand layer. *European Journal of Environmental and Civil Engineering*, 26, 3566-3582.

[19] Nainegali, L., Basudhar, P. K., & Ghosh, P. (2021). Interference of proposed footing with an existing footing resting on non-linearly elastic dense and loose cohesionless soil bed. *European Journal of Environmental and Civil Engineering*, 25, 2574-2591.

[20] Chavda, J.T. & Dodagoudar, G. (2021). On vertical bearing capacity of ring footings: Finite element analysis, observations and recommendations, *International Journal of Geotechnical Engineering*, 15(10), pp. 1207-1219

[21] Keawsawasvong, S., Thongchom, C. & Likitlersuang, S. (2021). Bearing capacity of strip footing on Hoek-brown rock mass subjected to eccentric and inclined loading. *Transportation Infrastructure Geotechnology*, 8(2), 189-202.

[22] Krabbenhoft, K., Lyamin, A., & Krabbenhoft, J. (2015). Optum computational engineering (OptumG2). Computer software.

[23] Sloan, S. (2013). Geotechnical stability analysis. *Géotechnique*, 63, 531-571.

[24] Buckingham, E. (1914). On physically similar systems; illustrations of the use of dimensional equations. *Physical review*, 4, 345.

[25] Davis, E. (1968). Theories of plasticity and the failure of soil masses. Soil mechanics: Selected topics, In Chapter 6, pp 341-380, American Elsevier New York.

Appendix A

L and C_u were selected as repeating variables, and φ, D, q_u and γ_g as nonrepeating variables. The friction angle (φ) was selected as the first dimensionless variable (π_1). So:

$$\pi_1 = \varphi \tag{A.1}$$

Then, the variable D was used to determine the second dimensionless variable (π_2). As a result:

$$\pi_2 = D.L^{\alpha}.C_u^{\beta} \tag{A.2}$$

As the above combination must not have any dimension, thus:

$$(\underline{L})(\underline{L}^{\alpha})(F\underline{L}^{-2})^{\beta} = \underline{L}^{0}F^{0} \tag{A.3}$$

Therefore:

$$1 + \alpha - 2\beta = 0 \tag{A.4}$$

and:

$$\beta = 0 \tag{A.5}$$

which led to $\alpha = -1$, and $\pi_2 = D/L$. Since L/D has been widely-used in the previous studies, the authors decided to substitute D/L with L/D for π_2.

In the next step, we considered q_u to obtain the third dimensionless variable (π_3) as follows:

$$\pi_3 = q_u.L^{\lambda}.C_u^{\gamma} \tag{A.6}$$

Hence:

$$(F\underline{L}^{-2})(\underline{L}^{\lambda})(F\underline{L}^{-2})^{\gamma} = F^{0}\underline{L}^{0} \tag{A.7}$$

As a result: $1 + \gamma = 0$, and $-2 + \lambda - 2\gamma = 0$. The resulting dimensionless product was:

$$\pi_3 = q_u/C_u \tag{A.8}$$

Finally, γ_g was used for obtaining the last dimensionless variable (π_4):

$$\pi_4 = \gamma_g.L^{a}.C_u^{b} \tag{A.9}$$

Since π_4 was dimensionless:

$$(F\underline{L}^{-3})(\underline{L}^{a})(F\underline{L}^{-2})^{b} = F^{0}\underline{L}^{0} \tag{A.10}$$

The above equation led to: $1 + b = 0$, and $-3 + a - 2b = 0$. Consequently: $a = 1$ and $b = -1$. Therefore:

$$\pi_4 = \frac{\gamma_g L}{C_u} \tag{A.11}$$

This article is an open-access article distributed under the terms and conditions of the Creative Commons Attribution (CC-BY) license.